npj computational materials

www.nature.com/npjcompumats

ARTICLE OPEN

Check for updates

Ferromagnetism and ferroelectricity in a superlattice of antiferromagnetic perovskite oxides without ferroelectric polarization

Paresh C. Rout[1,2], Avijeet Ray[1,2] and Udo Schwingenschlögl[1]✉

We study the structural, electronic, and magnetic properties of the $SrCrO_3/YCrO_3$ superlattice and their dependence on epitaxial strain. We discover that the superlattice adopts A-type antiferromagnetic (A-AFM) ordering in contrast to its constituents ($SrCrO_3$: C-AFM; $YCrO_3$: G-AFM) and retains it under compressive strain while becoming ferromagnetic (5 μ_B per formula unit) at +1% strain. The obtained ferroelectric polarization is significantly higher than that of the R_2NiMnO_6/La_2NiMnO_6 (R = Ce to Er) series of superlattices [*Nat. Commun.* 5, 4021 (2014)] due to a large difference between the antipolar displacements of the Sr and Y cations. The superlattice is a hybrid-improper multiferroic material with a spontaneous ferroelectric polarization (13.5 μC/cm^2) approaching that of bulk $BaTiO_3$ (19 μC/cm^2). The combination of ferromagnetism with ferroelectricity enables multistate memory applications. In addition, the charge-order-driven *p*-type semiconducting state of the ferromagnetic phase (despite the metallic nature of $SrCrO_3$) is a rare property and interesting for spintronics. Monte Carlo simulations demonstrate a magnetic critical temperature of 90 K for the A-AFM phase without strain and of 115 K for the ferromagnetic phase at +5% strain, for example.

npj Computational Materials (2023)9:165 ; https://doi.org/10.1038/s41524-023-01108-2

INTRODUCTION

Heterostructures of transition metal perovskites (ABO_3) provide a fertile ground to study emergent phenomena of correlated electrons and a promising route to new functional devices using quantum effects. Since the collective behavior of electrons at an oxide interface can differ strongly from that in the component materials, superlattices show a plethora of properties such as metal-to-insulator transition[1], high Néel temperature[2,3], formation of a two-dimensional electron gas[4], superconductivity[5], orientation-dependent magnetism[6,7], and charge-ordered ferroelectricity[8]. The presence of layers of A-site cations with different valence can induce charge and/or orbital ordering at the B-sites, which can lead to a ground state differing fundamentally from those of the component materials[8]. In addition, layer-by-layer deposition[9,10] offers the possibility to induce ferroelectric polarization in heterostructures of inversion-symmetric compounds[11].

$SrCrO_3$ is a metallic d^2 perovskite with the nonpolar tetragonal space group *P*4/mmm and C-type antiferromagnetic (C-AFM) ordering below the Néel temperature of 100 K[12]. It undergoes a metal-to-insulator transition under high pressure due to bond instability[13] and exhibits $d_{xy}^1 d_{xz}^{0.5} d_{yz}^{0.5}$ orbital ordering[14,15]. In a superlattice with $SrTiO_3$, it undergoes a metal-to-insulator transition under tensile strain due to a nonpolar-to-polar structural transition, inducing a ferroelectric polarization of 41 μC/cm^2 at +3% strain, for example, while adopting G-AFM ordering (zero magnetization)[12]. $YCrO_3$ is a semiconducting d^3 perovskite with the nonpolar orthorhombic space group *Pbnm*, G-AFM ordering below the Néel temperature of 141.5 K[16], and ferroelectric polarization of 2 μC/cm^2 due to off-centering of the Cr cations below 473 K[17]. While these results are based on polycrystalline samples, recently, high-quality single crystals have been synthesized at high temperatures, and crystal structure and magnetization measurements have been performed[18,19]. Single crystalline $YCrO_3$ shows a Néel temperature of 140 K and weak ferromagnetism at higher temperatures due to spin canting, combined with in-plane antiphase tilting and out-of-plane in-phase tilting of the O octahedra ($a^-a^-c^+$ tilting pattern in Glazer's notation)[18]. It is particularly interesting to explore the electronic and magnetic properties of the $SrCrO_3/YCrO_3$ superlattice, as both component materials lack magnetization and ferroelectric polarization while their electronic and magnetic properties can be controlled by strain engineering[20–23]. The average nominal valence of Cr is 3.5+ due to the Sr^{2+} and Y^{3+} states of the A-site cations. However, because of the strong Coulomb interaction, one may speculate that half of the Cr cations will realize a nominal valence of 3+ and the other half a nominal valence of 4+. As a result, a Mott-insulating state with charge, orbital, and/or magnetic ordering may be achieved.

Motivated by the new functionalities offered by superlattices and straintronics, we study the dependence of the multiferroic properties of the $SrCrO_3/YCrO_3$ superlattice under epitaxial strain. The superlattice turns out to be semiconducting despite the metallic nature of $SrCrO_3$. We show that magnetic states can be realized with large ferroelectric polarization despite the fact that the individual compounds show no ferroelectricity. The combination of large magnetization with large ferroelectric polarization gives rise to robust multiferroism, enabling multistate memory applications. Monte Carlo simulations are used to predict the critical temperatures of the magnetic phases.

RESULTS

First-principles calculations

We find that the $SrCrO_3/YCrO_3$ superlattice (Fig. 1a) adopts the monoclinic space group $P2_1$ due to a combination of the layered A-site cation ordering with an $a^-a^-c^+$ tilting pattern (like $YCrO_3$).

[1]Physical Sciences and Engineering Division (PSE), King Abdullah University of Science and Technology (KAUST), Thuwal 23955-6900, Saudi Arabia. [2]These authors contributed equally: Paresh C. Rout, Avijeet Ray. ✉email: udo.schwingenschlogl@kaust.edu.sa

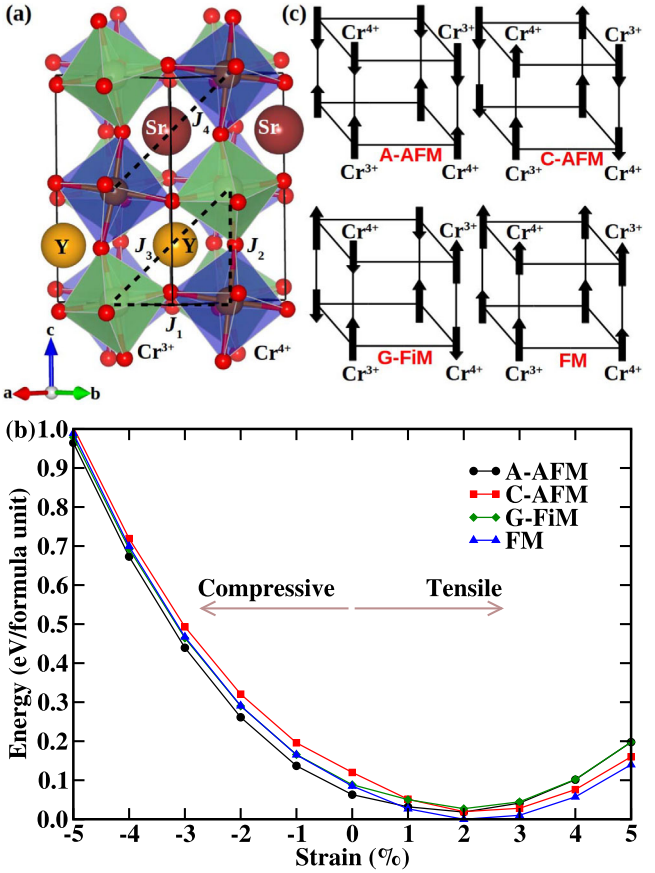

Fig. 1 Magnetic ordering. a Structure and exchange paths connecting the Cr^{3+} and Cr^{4+} ions, **b** strain dependence of the total energy, and **c** considered magnetic orderings.

The $P2_1$ symmetry is also obtained when we start the structure optimization from other possible $GdCrO_3$-type symmetries (space groups $Pna2_1$ and $Pca2_1$). We obtain A-AFM ordering without strain and a transition to FM ordering at +1% strain (Fig. 1b) with a large magnetization of 5 μ_B per formula unit. The occupation matrix and projected densities of states show that the superlattice adopts a checkerboard charge ordering with Cr^{3+} (d^3) and Cr^{4+} (d^2) states (Fig. 1c) throughout the considered range of strain. In other words, the nearest B-site neighbors of the Cr^{3+} ions are Cr^{4+} ions, and vice versa. This d^3-d^2 charge ordering creates a breathing distortion of the O octahedra with expansion around the Cr^{3+} ions and contraction around the Cr^{4+} ions, which is confirmed by the appearance of long and short bonds, respectively.

To understand the orbital occupations in detail, we investigate the projected densities of states, finding that in the spin-majority channel, the valence/conduction band edge is predominantly due to hybridized Cr^{3+}/Cr^{4+} 3*d* and O 2*p* orbitals (Fig. 2a), representing covalent Cr-O bonds. The presence of Y^{3+} ions distorts the O octahedra around the Cr^{4+} ions as compared to $SrCrO_3$, with four Cr-O bonds becoming shorter (1.89, 1.92, 1.96, and 1.98 Å instead of 2.05 Å). The bond lengths of the neighboring Cr^{3+} ions change slightly to accommodate these distortions but stay similar to those of $YCrO_3$. As a result of the modified bonding environment of the Cr^{4+} ions, the degenerate d_{xz} and d_{yz} states of $SrCrO_3$ (occupied by one electron) split such that the d_{xz} orbital carries one electron and the d_{yz} orbital remains empty, opening a small bandgap in the spin-majority channel (Fig. 2b). The electronic band structure indicates that the FM phase is an indirect narrow bandgap semiconductor (Fig. 2c).

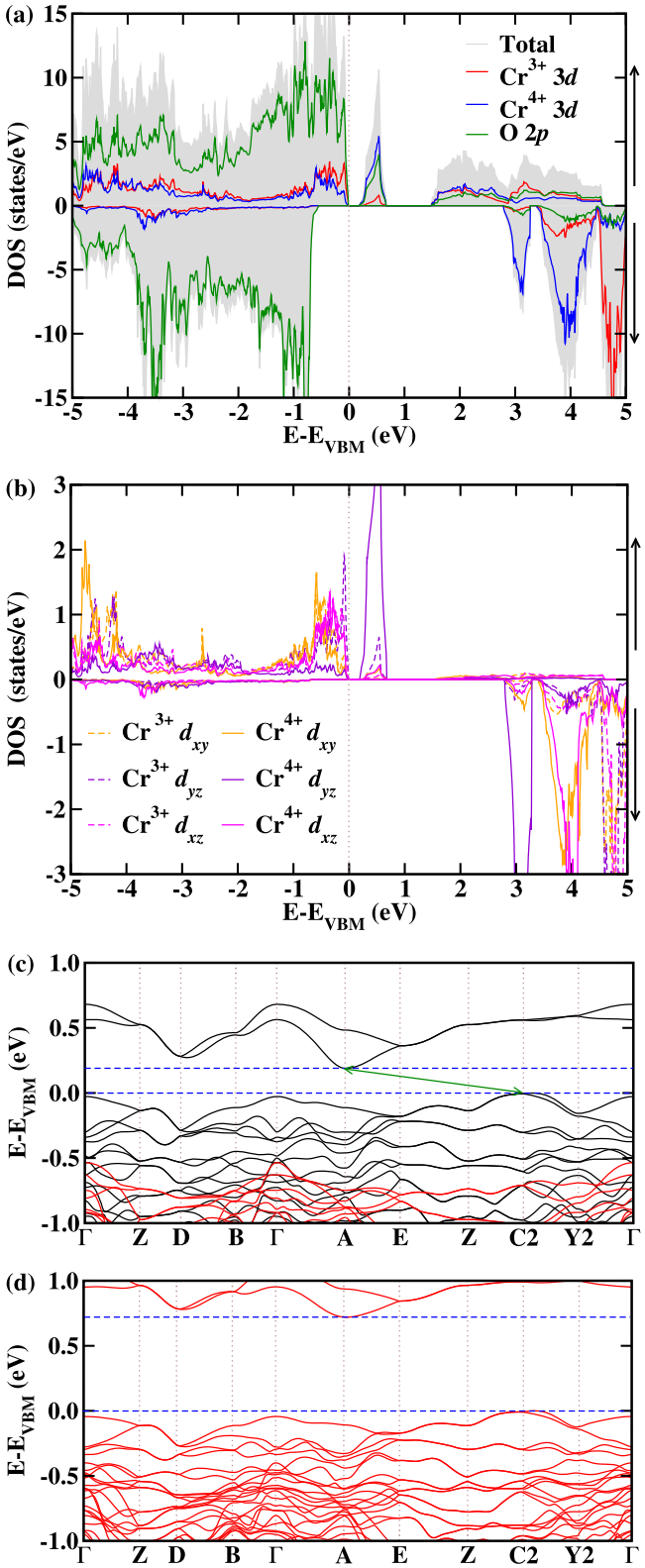

Fig. 2 FM phase. a, **b** Projected densities of states and **c** electronic band structure (black/red lines represent the spin-majority/spin-minority channel) of the FM phase at +5% strain. **d** Electronic band structure when the spin-orbit coupling is taken into account. Analogous results at +1% strain are shown in Supplementary Fig. 1.

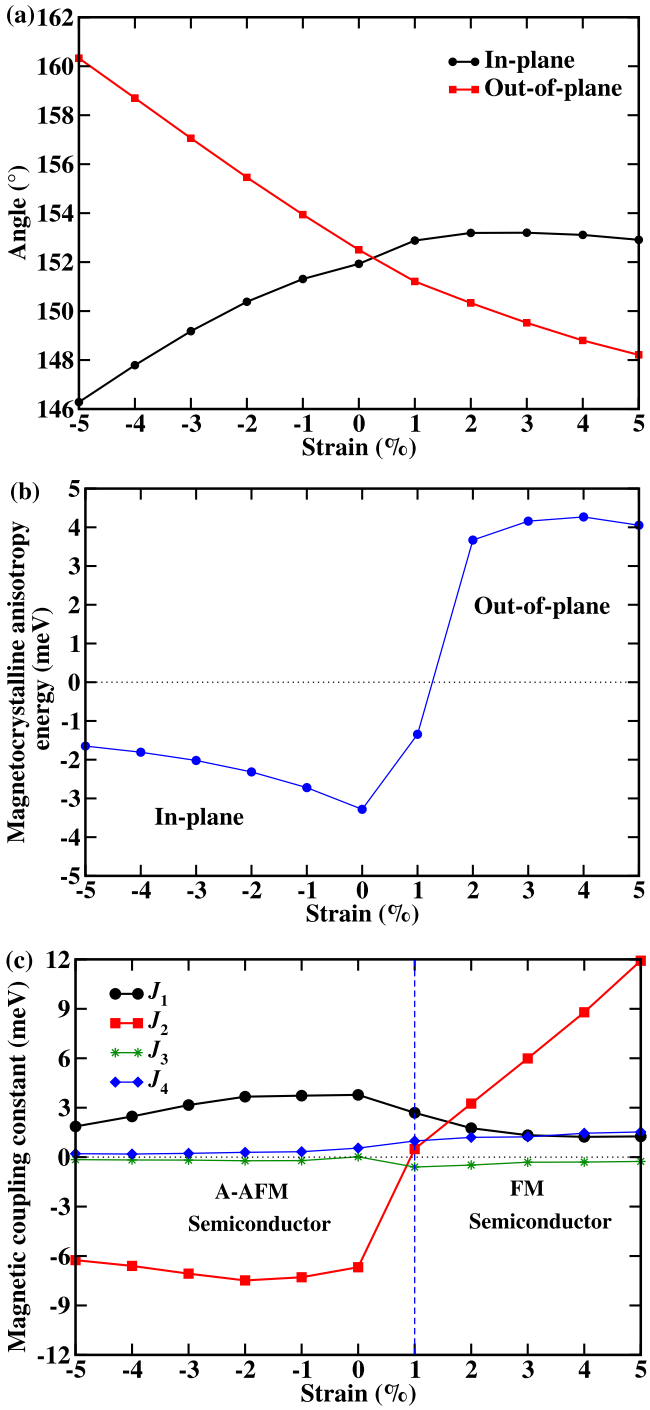

Fig. 3 Strain effects. Strain dependence of the **a** in-plane and out-of-plane Cr^{3+}-O-Cr^{4+} angles, **b** magnetocrystalline anisotropy energy, and **c** magnetic coupling constants.

While the superlattice realizes A-AFM ordering without strain and under compression, it realizes FM ordering under tension. To understand this observation, we measure the octahedral Cr^{3+}-O-Cr^{4+} angles (Fig. 3a). The in-plane angles of 146° to 153° result in FM in-plane exchange (Cr^{3+}-Cr^{4+}; Goodenough-Kanamori rules[24,25]). Under tension, the out-of-plane angles do not exceed the in-plane angles, and FM ordering is favored. Under compression, however, the out-of-plane angles exceed the in-plane angles, and the out-of-plane exchange becomes AFM, resulting in A-AFM ordering. We notice that the magnetocrystalline anisotropy switches from in-plane to out-of-plane between +1% and +2% strain (Fig. 3b).

Next, we extract the magnetic coupling constants using a Heisenberg spin Hamiltonian. We consider the in-plane nearest-neighbor coupling J_1, out-of-plane nearest-neighbor coupling J_2, and next-nearest-neighbor couplings J_3 and J_4 (Fig. 1a), assuming that the spin vectors are collinear with length one, as their magnitude later will be taken into account in the Monte Carlo simulations. The magnetic coupling constants are obtained by solving the coupled equations $E_1 = E_0 + 8J_1 - 4J_2 - 8J_3 - 8J_4$ (A-AFM), $E_2 = E_0 - 8J_1 + 4J_2 - 8J_3 - 8J_4$ (C-AFM), $E_3 = E_0 - 8J_1 - 4J_2 + 8J_3 + 8J_4$ (G-FiM), $E_4 = E_0 + 8J_1 + 4J_2 + 8J_3 + 8J_4$ (FM), $E_5 = E_0 + 8J_3 - 8J_4$ (G-FiM with one Cr^{3+} spin flipped), and $E_6 = E_0 - 8J_3 + 8J_4$ (G-FiM with one Cr^{4+} spin flipped), where E_0 is the lattice energy and E_1 to E_6 are the total energies of the magnetic orderings obtained from density functional theory. We find that J_1 is always positive (FM) while J_2 is negative (AFM) without strain and under compression but positive under tension. J_3 (Cr^{3+} to Cr^{3+}) is always slightly negative. J_4 (Cr^{4+} to Cr^{4+}) is slightly positive under compression, indicating a weak spin frustration, and slowly increases under tension to overtake J_1 between +3% and +4% strain (Fig. 3c), which is attributed to the decreasing out-of-plane Cr^{3+}-O-Cr^{4+} angles (Fig. 3a). The simultaneous increase of J_2 and J_4 is the prime reason for the A-AFM to FM transition. To compute the critical temperatures of the magnetic phases, we execute Monte Carlo simulations with Gaussian moves[26] for our Heisenberg model in a $12 \times 12 \times 12$ supercell, using 100,000 sweeps for thermalization and 80,000 additional sweeps for data collection. The Néel temperature of the A-AFM phase is found to be 90 K without strain and 50 K at −5% strain, for example, and the Curie temperature of the FM phase is found to be 115 K at +5% strain (Fig. 4).

We next turn to the projected densities of states and electronic band structure of the A-AFM phase at −5% strain (Fig. 5). In agreement with the zero magnetization, the densities of states of the two spin channels are identical. The orbital hybridizations at the valence and conduction band edges are the same as in the case of the FM phase, and we obtain an indirect narrow bandgap semiconductor again. While spin-orbit coupling was not included in previous studies of $SrCrO_3$ and $YCrO_3$ due to a minor impact on the electronic and magnetic properties[12,27], we find that in the case of the $SrCrO_3$/$YCrO_3$ superlattice, the bandgap increases significantly from 0.2 to 0.7 eV in the FM phase at +5% strain (Fig. 2d) and from 0.3 to 0.6 eV in the A-AFM phase at −5% strain (Fig. 5c), for example.

Since both the FM and A-AFM phases are semiconductors, we next calculate the ferroelectric polarization. Finite in-plane ferroelectric polarization results from unequal in-plane antipolar displacements of the Sr^{2+} and Y^{3+} cations due to their different ionic radii and oxidation states (Fig. 6a). We find differences of 0.032b, 0.028b, and 0.026b (0.16, 0.15, and 0.15 Å) at −5%, 0%, and +5% strain, respectively, which are much larger than those of the FM superlattices reported in ref. [11] due to the larger distortions of the O octahedra of the $SrCrO_3$/$YCrO_3$ superlattice. The obtained ferroelectric polarizations of 13.5, 12.1, and 11.0 μC/cm^2 along the *b*-axis (in-plane) at −5%, 0%, and +5% strain, respectively, correspondingly are much larger than those reported in ref. [11]. The antipolar displacements of the nearest-neighbor Sr^{2+} ions and of the nearest-neighbor Y^{3+} ions are equal along the *a*-axis, i.e., they do not result in ferroelectric polarization. The energy barrier to switch the ferroelectric polarization is found to be 0.27 eV at 0% strain (Fig. 6b).

DISCUSSION

In summary, we predict by first-principles calculations large hybrid-improper ferroelectric polarization for the superlattice composed of the perovskites $SrCrO_3$ and $YCrO_3$. A Cr^{3+}-Cr^{4+}

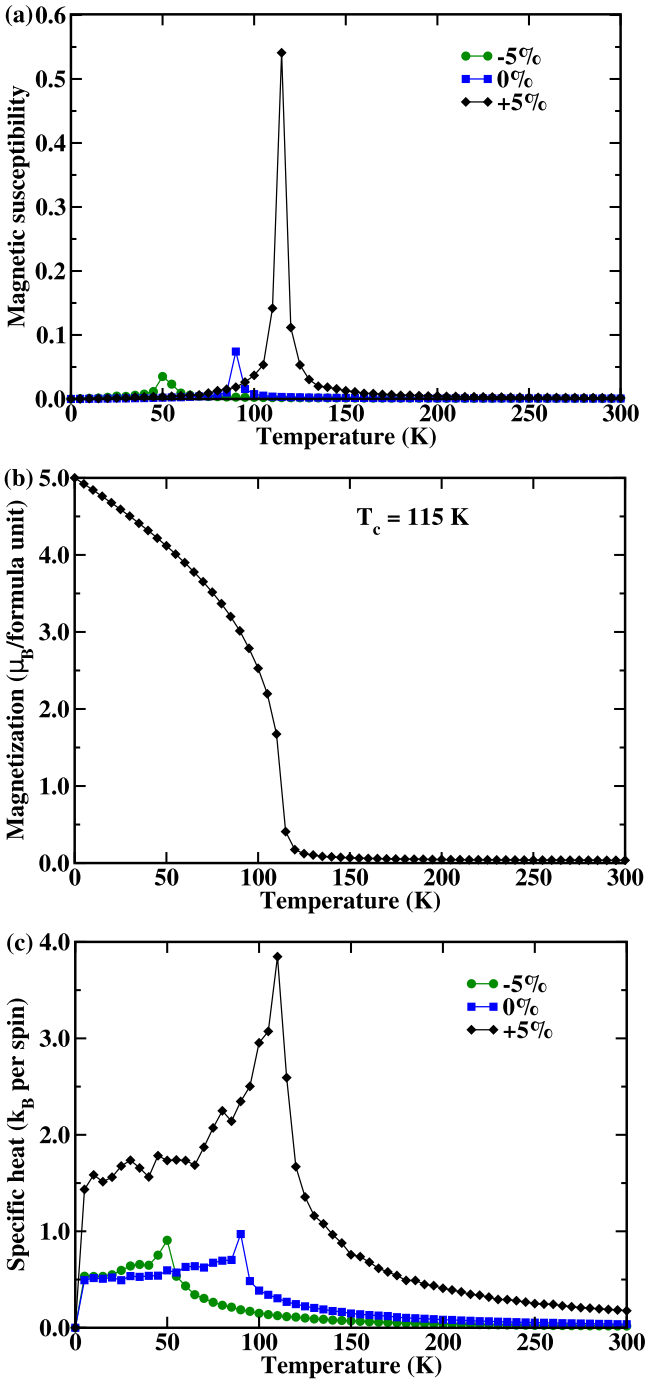

Fig. 4 Temperature effects. Temperature dependence of the **a** magnetic susceptibility at −5% (A-AFM phase), 0% (A-AFM phase), and +5% (FM phase) strain, with the peak marking the critical temperature, **b** magnetization at +5% strain when both the nearest-neighbor and next-nearest-neighbor couplings are considered, and **c** specific heat at −5%, 0%, and +5% strain.

checkerboard charge ordering is found without strain as well as under strain. We demonstrate that the formation of a superlattice is able to induce multiferroism even in perovskite oxides lacking both magnetism and ferroelectricity individually. The $SrCrO_3$/$YCrO_3$ superlattice adopts an A-AFM ordering without strain and under compression, while it becomes FM with a magnetization of 5 μ_B per formula unit at +1% strain. We find that the checkerboard charge ordering results in a band insulator with a narrow indirect bandgap. While FM metals are common, the combination of FM

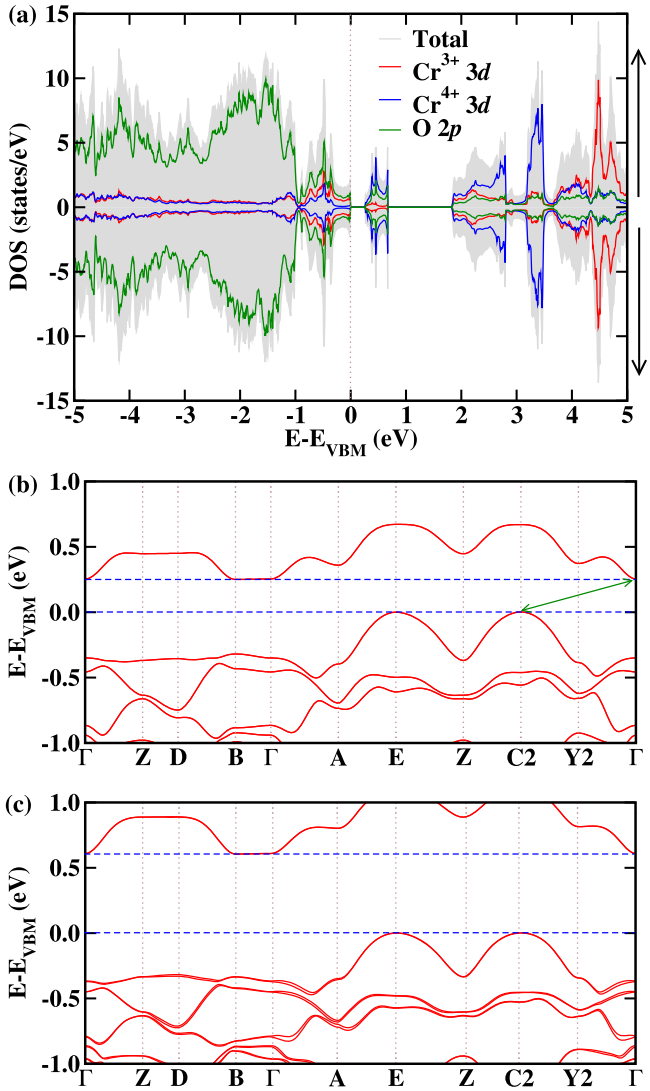

Fig. 5 A-AFM phase. a Projected densities of states and **b** electronic band structure of the A-AFM phase at −5% strain (spin channels degenerate). **c** Electronic band structure when the spin-orbit coupling is taken into account.

ordering with *p*-type semiconductivity is a rare phenomenon and interesting for spintronics applications. Monte Carlo simulations demonstrate magnetic critical temperatures of 50 K for the A-AFM phase at −5% strain and 115 K for the FM phase at +5% strain, for example. The hybrid-improper ferroelectric polarization is due to a large difference between the antipolar displacements of the Sr^{2+} and Y^{3+} cations (which can be controlled by strain) and its magnitude approaches that of conventional ferroelectric oxides such as $BaTiO_3$. Similar multiferroic phases can be expected to occur in superlattices with other transition metal ions that support multiple valence states.

METHODS

We perform first-principles calculations within the framework of density functional theory using the Quantum-ESPRESSO code[28]. The projector-augmented wave method and ultrasoft pseudopotentials are adopted. We employ the generalized gradient approximation of Perdew-Burke-Ernzerhof for the exchange-correlation functional and account for electronic correlations in the transition metal 3*d* orbitals by considering

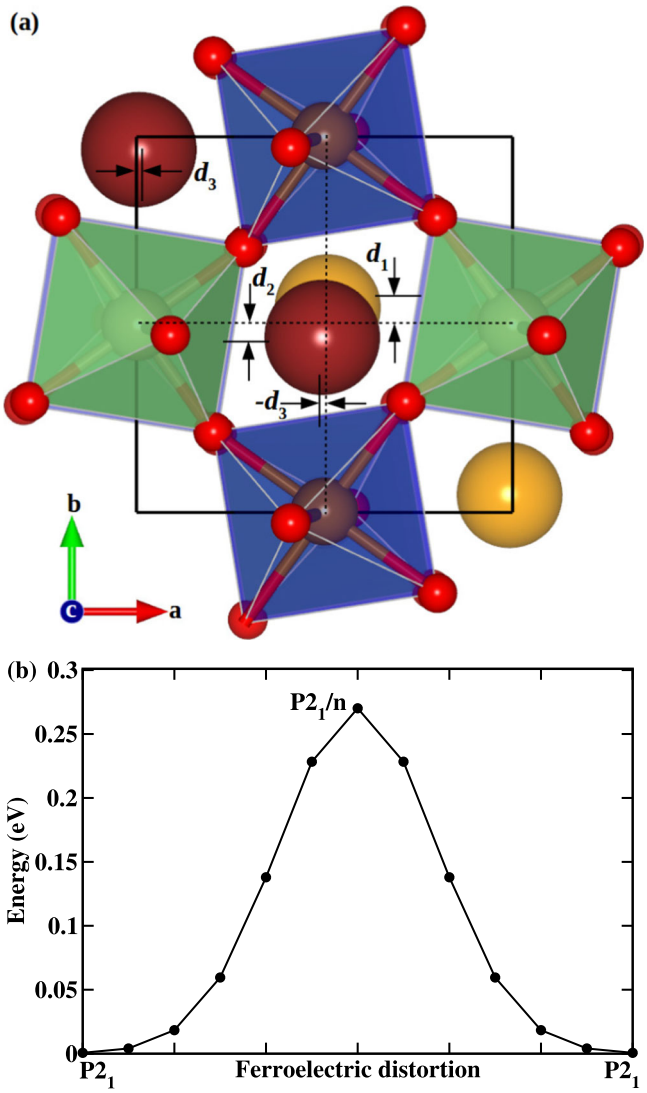

Fig. 6 Ferroelectric polarization. a In-plane antipolar displacements and **b** energy barrier to switch the ferroelectric polarization at 0% strain.

an onsite Coulomb interaction[29] of the established literature value of 4 eV, which reproduces the experimental lattice constants of $SrCrO_3$ (experiment: 3.87 Å; theory: 3.81 Å)[14] and $YCrO_3$ (experiment: 3.84 Å; theory: 3.79 Å)[18,30]. We have checked that the magnetic ground state of the superlattice does not change for onsite Coulomb interactions of 2, 3, and 5 eV. A cutoff of 90 Ry is used for the plane waves and a cutoff of 640 Ry for the augmentation charge. The Brillouin zone is sampled on an $8\times8\times6$ Monkhorst-Pack k-mesh in the structure optimization, which is found to provide convergence of the total energy, and on a $14\times14\times12$ Monkhorst-Pack k-mesh in the calculation of the electronic band structure and density of states. The total energy convergence criterion is set to 10^{-8} Ry. All structures are optimized until the Hellmann-Feynman forces stay below 10^{-5} Ry/Bohr. The ferroelectric polarization is calculated by the Berry phase approach[31] on a $10\times50\times10$ Monkhorst-Pack k-mesh to achieve convergence.

We set the in-plane lattice constants of $SrCrO_3$ and $YCrO_3$ equal ($a = b = 3.80$ Å) to mimic (001) epitaxial growth. The length and angle of the out-of-plane lattice vector are optimized for each strain value simultaneously with the atomic positions. This procedure is executed for different magnetic orderings to capture the strain effect on the relative energies of these orderings. Since $SrCrO_3$ and $YCrO_3$ have a lattice mismatch of only 0.5% (lattice constants of 3.81 and 3.79 Å, respectively), realization of a 1:1 superlattice is experimentally feasible thanks to recent developments in layer-by-layer deposition techniques[10].

DATA AVAILABILITY

The data generated in this study are available on request from the authors.

Received: 17 February 2023; Accepted: 2 August 2023;
Published online: 07 September 2023

REFERENCES

1. Dong, S. et al. Magnetism, conductivity, and orbital order in $(LaMnO_3)_{2n}/(SrMnO_3)_n$ superlattices. *Phys. Rev. B* **78**, 201102 (2008).
2. May, S. J. et al. Enhanced ordering temperatures in antiferromagnetic manganite superlattices. *Nat. Mater.* **8**, 892–897 (2009).
3. Nanda, B. R. K. & Satpathy, S. Effects of strain on orbital ordering and magnetism at perovskite oxide interfaces: $LaMnO_3/SrMnO_3$. *Phys. Rev. B* **78**, 054427 (2008).
4. Ohtomo, A. & Hwang, H. Y. A high-mobility electron gas at the $LaAlO_3/SrTiO_3$ heterointerface. *Nature* **427**, 423–426 (2004).
5. Nakagawa, N., Hwang, H. Y. & Muller, D. A. Why some interfaces cannot be sharp. *Nat. Mater.* **5**, 204–209 (2006).
6. Gibert, M., Zubko, P., Scherwitzl, R., Íñiguez, J. & Triscone, J.-M. Exchange bias in $LaNiO_3$-$LaMnO_3$ superlattices. *Nat. Mater.* **11**, 195–198 (2012).
7. Dong, S. & Dagotto, E. Quantum confinement induced magnetism in $LaNiO_3$-$LaMnO_3$ superlattices. *Phys. Rev. B* **87**, 195116 (2013).
8. Park, S. Y., Kumar, A. & Rabe, K. M. Charge-order-induced ferroelectricity in $LaVO_3/SrVO_3$ superlattices. *Phys. Rev. Lett.* **118**, 087602 (2017).
9. Hwang, H. Y. et al. Emergent phenomena at oxide interfaces. *Nat. Mater.* **11**, 103–113 (2012).
10. Lei, Q. et al. Constructing oxide interfaces and heterostructures by atomic layer-by-layer laser molecular beam epitaxy. *NPJ Quantum Mater.* **2**, 10 (2017).
11. Zhao, H. J. et al. Near room-temperature multiferroic materials with tunable ferromagnetic and electrical properties. *Nat. Commun.* **5**, 4021 (2014).
12. Zhou, Y. & Rabe, K. M. Coupled nonpolar-polar metal-insulator transition in 1:1 $SrCrO_3/SrTiO_3$ superlattices: a first-principles study. *Phys. Rev. Lett.* **115**, 106401 (2015).
13. Zhou, J.-S., Jin, C.-Q., Long, Y.-W., Yang, L.-X. & Goodenough, J. B. Anomalous electronic state in $CaCrO_3$ and $SrCrO_3$. *Phys. Rev. Lett.* **96**, 046408 (2006).
14. Ortega-San-Martin, L. et al. Microstrain sensitivity of orbital and electronic phase separation in $SrCrO_3$. *Phys. Rev. Lett.* **99**, 255701 (2007).
15. Lee, K.-W. & Pickett, W. E. Orbital-ordering driven structural distortion in metallic $SrCrO_3$. *Phys. Rev. B* **80**, 125133 (2009).
16. Looby, J. T. & Katz, L. Yttrium chromium oxide, a new compound of the perovskite type. *J. Am. Chem. Soc.* **76**, 6029–6030 (1954).
17. Serrao, C. R., Kundu, A. K., Krupanidhi, S. B., Waghmare, U. V. & Rao, C. N. R. Biferroic $YCrO_3$. *Phys. Rev. B* **72**, 220101 (2005).
18. Zhu, Y. et al. High-temperature magnetism and crystallography of a $YCrO_3$ single crystal. *Phys. Rev. B* **101**, 014114 (2020).
19. Zhu, Y. et al. Crystalline and magnetic structures, magnetization, heat capacity, and anisotropic magnetostriction effect in a yttrium-chromium oxide. *Phys. Rev. Mater.* **4**, 094409 (2020).
20. Dupé, B., Prosandeev, S., Geneste, G., Dkhil, B. & Bellaiche, L. $BiFeO_3$ films under tensile epitaxial strain from first principles. *Phys. Rev. Lett.* **106**, 237601 (2011).
21. Escorihuela-Sayalero, C., Diéguez, O. & Íñiguez, J. Strain engineering magnetic frustration in perovskite oxide thin films. *Phys. Rev. Lett.* **109**, 247202 (2012).
22. Lu, X.-Z. & Rondinelli, J. M. Epitaxial-strain-induced polar-to-nonpolar transitions in layered oxides. *Nat. Mater.* **15**, 951–955 (2016).
23. Rout, P. C. & Schwingenschlögl, U. Strain-attenuated spin frustration in double perovskite Sr_2FeOsO_6. *Phys. Rev. B* **103**, 024426 (2021).
24. Goodenough, J. B. *Magnetism and Chemical Bond: Electronic Structure, Exchange and Magnetism in Oxides* (Interscience, 1963).
25. Kanamori, J. Superexchange interaction and symmetry properties of electron orbitals. *J. Phys. Chem. Solids* **10**, 87–98 (1959).
26. Evans, R. F. L. et al. Atomistic spin model simulations of magnetic nanomaterials. *J. Phys. Condens. Matter* **26**, 103202 (2014).
27. Bhowmik, T. K. & Sinha, T. P. Al-dependent electronic and magnetic properties of $YCrO_3$ with magnetocaloric application: an ab-initio and Monte Carlo approach. *Phys. B Condens. Matter* **606**, 412659 (2021).

28. Giannozzi, P. et al. QUANTUM ESPRESSO: a modular and open-source software project for quantum simulations of materials. *J. Phys. Condens. Matter* **21**, 395502 (2006).
29. Anisimov, V. I., Aryasetiawan, F. & Liechtenstein, A. I. First-principles calculations of the electronic structure and spectra of strongly correlated systems: the LDA+U method. *J. Phys. Condens. Matter* **9**, 767–808 (1997).
30. Sardar, K., Lees, R. M., Kashtiban, J. R., Sloan, J. & Walton, R. I. Direct hydrothermal synthesis and physical properties of rare-earth and yttrium orthochromite perovskites. *Chem. Mater.* **23**, 48–56 (2011).
31. King-Smith, R. D. & Vanderbilt, D. Theory of polarization of crystalline solids. *Phys. Rev. B* **47**, 1651–1654 (1993).

ACKNOWLEDGEMENTS

The research reported in this publication was supported by funding from King Abdullah University of Science and Technology (KAUST). For computer time, this research used the resources of the Supercomputing Laboratory at KAUST.

AUTHOR CONTRIBUTIONS

P.C.R. and A.R. conducted the calculations. All authors contributed to the interpretation of the data and writing of the manuscript.

COMPETING INTERESTS

The authors declare no competing interests.

ADDITIONAL INFORMATION

Supplementary information The online version contains supplementary material available at https://doi.org/10.1038/s41524-023-01108-2.

Correspondence and requests for materials should be addressed to Udo Schwingenschlögl.

Reprints and permission information is available at http://www.nature.com/reprints

Publisher's note Springer Nature remains neutral with regard to jurisdictional claims in published maps and institutional affiliations.